

Particle concentration evolution and sedimentation-induced instabilities in a stably stratified environment

François Blanchette^{a)} and John W. M. Bush

Department of Mathematics, Massachusetts Institute of Technology, 77 Massachusetts Avenue, Cambridge, Massachusetts 02139

(Received 21 May 2004; accepted 5 May 2005; published online 24 June 2005)

We present the results of a combined experimental and theoretical investigation of sedimentation in a stratified fluid. The theory of sedimentation in a homogeneous ambient is extended to include the influence of a spatially varying particle settling speed. The results of an experimental investigation of latex particles settling in a stably stratified salt water solution are reported. Density variations in the suspending fluid reduce the particle settling speed which increases particle concentrations, thus enhancing the effects of hindered settling. A criterion is developed for the convective instability of an initially uniform suspension settling in a stably stratified ambient. If, as depth increases, the magnitude of the ambient density gradient decreases sufficiently rapidly, an initially uniform particle concentration will give rise to a statically unstable density profile. Experimental observations provide qualitative verification of this new stability criterion. © 2005 American Institute of Physics. [DOI: 10.1063/1.1947987]

I. INTRODUCTION

Sedimentation in stratified fluids is a problem of primary environmental importance. Suspensions arise in a variety of natural forms, including dust particles in the atmosphere,¹ sediment in rivers and oceans,² and crystals in magma chambers.³ Particle settling is particularly significant in the dynamics of coastal currents² and fluvial plumes in stratified estuaries.⁴ Ambient stratification may also influence the dynamics of microorganisms in the oceans.⁵ The interaction of particulate matter and density gradients also arises in a wide variety of industrial settings including the dispersal of pollutants in the atmosphere,⁶ the dilution of undersea sewage clouds,⁷ and the dumping of dredged materials.⁸

In general, the speed of a settling particle may vary as a result of changes in ambient density, viscosity, particle size, or body force. For example, stable density gradients are common in the ocean owing to vertical variations in temperature and salinity. The influence of vertical viscosity gradients on particle settling speed may be important for crystals settling in magma chambers.⁹ Significant particle size changes may arise in the melting or formation of ice crystals in frazil ice¹⁰ and during the sedimentation of crystals in magma.¹¹ The size of bubbles may also increase as they rise in the presence of a pressure gradient.¹² Alternatively, settling speeds may vary due to spatial gradients in the applied body force; for example, in centrifugation processes, the centrifugal force and particle speed necessarily increase with distance to the rotation axis.¹³

The settling speed, u_s , of low Reynolds number spherical particles, $Re_p = u_s a / \nu \ll 1$, in a suspension with particle volume fraction ϕ , is typically written as

$$u_s = f(\phi) U_s = f(\phi) \frac{2a^2 g (\rho_p - \rho_f)}{9\nu\rho_f}, \quad (1)$$

where U_s is the Stokes settling speed of a single particle in an unbounded ambient, a the particle radius, ν the kinematic viscosity, g the gravitational acceleration, and ρ_p and ρ_f the particle and fluid densities, respectively.¹⁴ Hindered settling is the reduction of the settling speed of an individual particle due to a combination of hydrodynamic forces between neighboring particles and upward motion of the ambient fluid displaced by the particles, the so-called fluid reflux.¹⁵ The average settling speed is reduced as the concentration increases so that $f(\phi) \leq 1$ and $f'(\phi) < 0$. The direct summing of the contribution of neighboring particles to the velocity of an individual particle is divergent, but this problem was circumvented by Batchelor,¹⁶ who used a renormalization method to demonstrate that in the limit of small particle concentrations, $f(\phi) = 1 - 6.55\phi + O(\phi^2)$. A commonly accepted empirical formula inferred for moderate values of ϕ ($0 < \phi < 15\%$) is that of Richardson and Zaki:¹⁷

$$f(\phi) = (1 - \phi)^n \quad n = 5.1 \pm 0.1. \quad (2)$$

We here examine the influence of vertical gradients in settling speed on the evolution of a suspension. For the sake of comparison with experiments, we focus on the effects of vertical density gradients. As a measure of the magnitude of the settling speed variation, we consider the relative velocity variation $\gamma = (u_h - u_0) / u_0$, where u_h and u_0 are, respectively, the Stokes settling speed at the top and bottom of the suspension. When settling speed variations arise only from density gradients, γ reduces to

$$\gamma = \frac{\rho_0 - \rho_h}{\rho_p - \rho_0}, \quad (3)$$

with ρ_h and ρ_0 the density at the top and bottom of the suspension, respectively. Particles having a density close to

^{a)} Author to whom correspondence should be addressed. Present address: James Franck Institute, University of Chicago, 5640 S. Ellis Ave., Chicago, IL 60637. Electronic mail: blanchef@uchicago.edu

that of the ambient fluid are thus subject to relatively large velocity variations.

The influence of a stable ambient density gradient on the settling speed of a single low Reynolds number particle was studied by Oster,¹⁸ who demonstrated that the settling speed adjusts to the surrounding conditions on a time scale $t_a \sim a^2/\nu$. The ratio of the adjustment time to the time required for a particle to settle a distance equal to its radius, $t_s = a/U_s$, is thus equal to the particle Reynolds number, $\text{Re}_p = U_s a/\nu$. We here focus our attention on particle settling for which $\text{Re}_p \ll 1$, which allows us to assume that the settling speed adjusts instantaneously and thus depends only on local parameters; Eq. (2) thus remains valid.

Instabilities may develop in a sedimenting system if a region of high particle concentration overlies a particle-depleted region. Details of the instability of a region of high sand concentration settling into a clear fluid in a vertical Hele-Shaw cell were recently investigated by Völtz, Pesch, and Rehberg¹⁹ and many similarities with the classic Rayleigh-Taylor instability were observed. A similar instability may result from particles settling across an ambient density jump. If a particle-laden fluid overlies a heavier, particle-free fluid, the initial density profile may be stable; however, as particles settle across the density interface, they form a region of high concentration above a particle-free region. The resulting three-layer system may then become unstable and the form of the resulting instabilities has been examined by Hoyal, Bursik, and Atkinson,²⁰ and Parsons, Bush, and Syvitski.²¹

As particles settle, random particle concentration fluctuations generally occur, leading to large-scale density gradients and concomitant convective motions.²² Such concentration variations occur on the scale of the container size, h , and scale as $\Delta\phi_f \sim (\phi a^3/h^3)^{1/2}$, thus giving rise to convective motions of typical velocity $U_f \sim g'(\phi a^3 h)^{1/2}/\nu$, where $g' = g(\rho_p - \rho_f)/\rho_f$ is the reduced buoyancy of particles.²³ Particle mass conservation requires that the settling of particles through an ambient density gradient generate particle concentration variations with characteristic scale $\Delta\phi_s \sim \phi \Delta\rho_f/\rho$, where $\Delta\rho_f$ is a typical ambient density variation. These may give rise to convective motions on the scale of the container size with typical velocity $U_c \sim g(\Delta\rho_f/\rho)h^2/\nu$.²⁴ We restrict our study to systems where the size of particles ($\sim 10^{-5}$ m) and of the container ($\sim 10^{-1}$ m) are such that $\Delta\phi_f \sim 10^{-7}$ is small relative to both $\phi \sim 10^{-2}$ and $\Delta\phi_s \sim 10^{-4}$ and we may thus neglect the effect of random fluctuations.

We begin by extending the description of hindered settling in a homogeneous fluid¹⁵ to the case of a stably stratified ambient in Sec. II. The stability of the resulting motion is discussed in Sec. III. In Sec. IV we present the results of an experimental investigation of latex particles settling in a density gradient and compare them with the theoretical descriptions of Secs. II and III.

II. THEORETICAL DEVELOPMENTS

We consider the equation of conservation of particles in the absence of fluid motion

$$\partial_t \phi - \partial_z(u_s \phi) = 0. \quad (4)$$

Here t and z , respectively, denote time and height, taken to be increasing upward. The relative importance of particle settling and diffusion of particle concentration due to hydrodynamic dispersion is prescribed by the Péclet number, $\text{Pe} = u_s h/\kappa_\phi$, with κ_ϕ the diffusion coefficient of particles and h the height of the container. We consider the large Péclet number limit in which particle diffusion may be neglected; moreover, we focus on suspensions where the particle size is sufficiently large that Brownian motion of particles is negligible. We assume that the particle settling speed and concentration are uniform in any horizontal plane so that we can restrict our domain to one spatial dimension. The hyperbolic conservation model (4) is expected to adequately describe the particle concentration evolution everywhere except in thin regions of characteristic scale h/Pe adjoining concentration discontinuities, where the effects of hydrodynamic dispersion may become important. Previous experimental work has confirmed the validity of the hyperbolic model in describing sedimentation in constant density ambients for both continuous and discontinuous particle concentration profiles.^{25,26}

The development of convective instabilities that violate the horizontal uniformity condition will be considered in Sec. III. We assume the settling speed to be of the form (1). We consider monodisperse suspensions and low particle concentrations ($\phi \ll 1$) so that the fluid reflux is weak ($u_r \sim u_s \phi$) and may be neglected. We thus have that $U_s(z)$ is time independent and find

$$\partial_t \phi - U_s V(\phi) \partial_z \phi = \phi f(\phi) \partial_z U_s \quad (5)$$

where

$$V(\phi) = \frac{d}{d\phi}(\phi f(\phi)). \quad (6)$$

Using the method of characteristics (e.g., Debnath²⁷), we observe that solving (5) is equivalent to solving simultaneously

$$dt = -\frac{1}{U_s} \frac{dz}{V(\phi)} = \frac{d\phi}{\phi f(\phi) \partial_z U_s}. \quad (7)$$

In general, this system cannot be solved analytically; however, special cases may be investigated in detail.

A. Homogeneous ambient

We first restrict our attention to homogeneous ambients where u_s depends exclusively on ϕ . In this limit, Kynch¹⁵ showed that the concentration of particles remains constant along straight lines in the time-height plane described by

$$\frac{dz}{dt} = -U_s V(\phi). \quad (8)$$

Note that for small values of ϕ , approximately below 15%, $V(\phi)$ is positive and decreasing.¹⁷ Given an initial particle concentration, one may thus plot the associated characteristics and deduce the concentration at later times.

Two notable complications may occur; the first results from divergent characteristics. Consider an initial profile

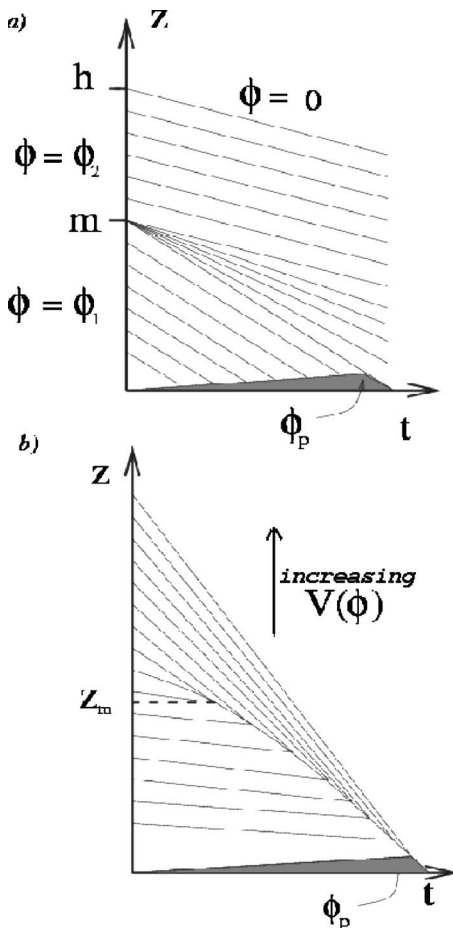


FIG. 1. Schematic illustration of the evolution of particle concentration along characteristics in a homogeneous ambient. (a) If $V(\phi_2) < V(\phi_1)$, with $V(\phi) = d(\phi f(\phi)) / d\phi$, characteristics travel faster in the underlying region ($z < m$) and an expansion fan forms from an initial discontinuity in particle concentration. (b) If $V(\phi)$ increases with z , a shock may develop from a continuous initial distribution. The bottom region shows the accumulation of particles at their packing concentration, ϕ_p .

where the concentration below $z = m$ is given by ϕ_1 and that above by ϕ_2 , as shown in Fig. 1(a). If the slope of characteristics associated with ϕ_2 is greater than that associated with ϕ_1 (i.e., $-U_s V(\phi_2) \geq -U_s V(\phi_1)$), no characteristics will pass through a region of the tz -plane with apex at the point ($t=0, z=m$). For low particle concentrations ($\leq 15\%$), this corresponds to cases where $\phi_1 < \phi_2$. An expansion fan then forms and matches continuously the two regions of known uniform concentration. The concentration at any point in the expansion fan, $\phi_e(t, z)$, satisfies

$$z - m = -U_s V(\phi_e) t. \tag{9}$$

If instead characteristics are converging, discontinuities in the particle concentration will form, see Fig. 1(b). When two characteristics meet, the concentration of particles cannot be found through the use of Eq. (4) alone. Because the concentration becomes discontinuous, a discrete expression for the particle conservation is needed to track the progression of the discontinuity. Labeling the region above the jump with index a and the region below with index b , conservation of particles then requires $\phi_a (U_s f(\phi_a) + U_j) = \phi_b (U_s f(\phi_b) + U_j)$,

where U_j is the propagation speed of the jump. The shock thus moves through the suspension with speed

$$U_j = -U_s \frac{\phi_b f(\phi_b) - \phi_a f(\phi_a)}{\phi_b - \phi_a} \tag{10}$$

provided $V(\phi_a) > V(\phi_b)$; otherwise, no discontinuities form. Note that shocks typically form when $\phi_a < \phi_b$, thus ensuring that they remain stable and do not generate convective motions. Concentration jumps may also form from continuous initial particle distributions when $dV(\phi)/dz$ becomes infinite. Characteristics then cross and the time evolution of the concentration is found by following characteristics until they form a shock, and subsequently tracking the position of the shock using Eq. (10), as shown schematically in Fig. 1(b). If the initial particle concentration is continuous, the characteristics that first meet originate from points infinitesimally close, which we denote by z_0 and $z_0 + \epsilon$, with $\epsilon \rightarrow 0$. Denoting the initial particle distribution by $\phi_i(z)$, the time, t_j , at which characteristics originating from z_0 and $z_0 + \epsilon$ intersect satisfies

$$z_0 - U_s V(\phi_i(z_0)) t_j = z_0 + \epsilon - U_s V(\phi_i(z_0 + \epsilon))$$

Taking the limit $\epsilon \rightarrow 0$ and denoting the maximum of $dV(\phi_i)/dz$ by z_m indicates that characteristics first cross at

$$t_j = \frac{1}{U_s} \frac{1}{\left. \frac{dV(\phi_i)}{dz} \right|_{z_m}} \quad z_j = z_m - \frac{V(\phi_i(z_m))}{\left. \frac{dV(\phi_i)}{dz} \right|_{z_m}}.$$

As particles reach the bottom of the container, their concentration reaches a maximum approximately equal to the close-packed concentration²⁸ $\phi_p \sim 0.62$. The bottom of the container is thus a source of characteristics of slope $-U_s V(\phi_p)$. Note that these lines are expected to have a positive slope corresponding to the accumulation of particles at the bottom. Similarly, characteristics of slope $-U_s V(0)$ originate from the top of the suspension if no new particles are introduced. In a homogeneous ambient, these upper and lower boundary conditions are sufficient to track the evolution of ϕ throughout the suspension.

B. Stratified ambient

We now consider particles settling through an ambient in which the settling speed of individual particles decreases linearly from u_h at the top, $z=h$, to u_0 at the bottom, $z=0$, due to some combination of density, viscosity, or body force variations. The settling speed of particles within the suspension is then of the form $u_s(z, \phi) = f(\phi)(u_0 + \Gamma z)$, where the velocity gradient is $\Gamma = (u_h - u_0)/h$. The system (7) then takes the form

$$dt = - \frac{dz}{(u_0 + \Gamma z)V(\phi)} = \frac{1}{\Gamma f(\phi)\phi} \frac{d\phi}{\phi}. \tag{11}$$

Solving for the first and third terms, and for the second and third terms yields, respectively,

$$K_1 = P(\phi) - \Gamma t, \quad K_2 = \phi f(\phi) U_s \tag{12}$$

where we define $P(\phi) = \int_{1/2}^{\phi} dc / (cf(c))$ and K_1, K_2 are constants. The general solution is thus

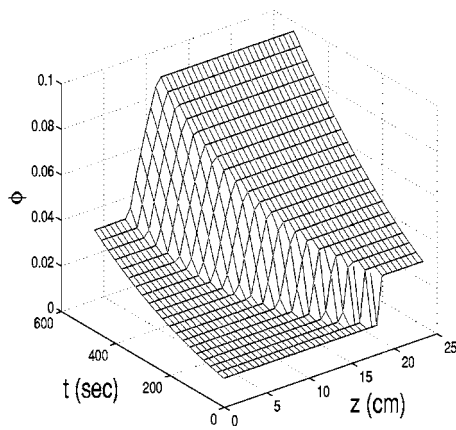


FIG. 2. The time evolution of an initial particle concentration jump of particles of radius $50 \mu\text{m}$ and density 1.19 g/cc settling in a stable linear density gradient, with density 1 g/cc at the top and 1.18 g/cc at the bottom, as computed via Eqs. (14) and (15). Here initial particle concentrations are $\phi_1=0.01$ below $z=20 \text{ cm}$ and $\phi_2=0.03$ above $z=20 \text{ cm}$. Characteristics are divergent, leading to the formation of an expansion fan.

$$\Gamma t = P(\phi) + F(U_s \phi f(\phi)) \quad (13)$$

In general, this solution may only be expressed implicitly, but simple initial conditions yield explicit expressions.

We consider a step function as an initial condition: $\phi = \phi_1$ if $0 < z < m$, $\phi = \phi_2$ if $m < z < h$ and $\phi = 0$ otherwise, as shown in Fig. 1(a). Characteristics are described by $dz/dt = -(u_0 + \Gamma z)V(\phi)$ and for general ϕ_1 and ϕ_2 , the particle concentration satisfies

$$\phi(z, t) = P^{-1}(\Gamma t + P(\phi_1)) = P^{-1}(\Gamma t + P(\phi_2)) \quad (14)$$

We consider the function $V(\phi)$ to be decreasing with ϕ , a dependence that has been verified experimentally for low particle concentrations ($\phi \leq 15\%$) by Richardson and Zaki.¹⁷ If $\phi_1 < \phi_2$, the regions of concentration $P^{-1}(\Gamma t + P(\phi_1))$ and $P^{-1}(\Gamma t + P(\phi_2))$ drift apart and are joined by an expansion fan. For any point (z, t) in that region, $\phi(z, t) = P^{-1}(\Gamma t + P(\phi_m))$, where ϕ_m satisfies

$$m = \frac{1}{\Gamma} \left[\frac{P^{-1}(\Gamma t + P(\phi_m)) f(P^{-1}(\Gamma t + P(\phi_m)))}{\phi_m f(\phi_m)} (u_0 + \Gamma z) - u_0 \right]. \quad (15)$$

Because $dV(\phi)/d\phi < 0$, we must have that $\phi_1 < \phi_m < \phi_2$; the concentration of the suspension may thus be determined everywhere. Using the Richardson-Zaki formula (2) allows us to compute the concentration evolution numerically. Figure 2 illustrates the evolution of a particle concentration jump with $\phi_1 < \phi_2$ settling in a stable linearly stratified ambient. The position of the top interface z_i may be found by integrating

$$\frac{dz_i}{dt} = f(\phi)(u_0 + \Gamma z_i) \quad (16)$$

with the initial condition $z_i(0) = h$.

If $\phi_1 > \phi_2$, the two regions described by Eq. (14) overlap, leading to the formation of a shock across which the concentration changes abruptly. The presence of a disconti-

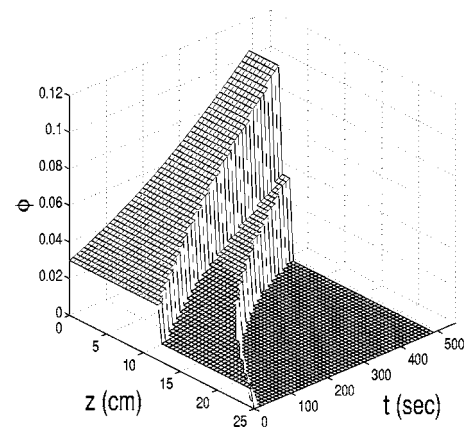


FIG. 3. Time evolution of a concentration jump of particles of radius $50 \mu\text{m}$ and density 1.19 g/cc settling in a stable linear density gradient, with density 1 g/cc at the top and 1.18 g/cc at the bottom, computed via Eqs. (14) and (17). Initial concentrations are $\phi_1=0.03$ below $z=12 \text{ cm}$ and $\phi_2=0.01$ above $z=12 \text{ cm}$. Characteristics are convergent, thus the concentration jump remains sharp. The rate of descent of the upper interface and concentration jump are markedly different.

nity again forces the use of a discrete statement of particle conservation from which we deduce that the concentration jump propagates with speed U_j given by

$$U_j(z, t) = \frac{dz_j}{dt} = U_s(z) \frac{\phi_b f(\phi_b) - \phi_a f(\phi_a)}{\phi_b - \phi_a} \quad (17)$$

The position of the shock, z_j , may thus be obtained by integrating equation (17) in time. Using the Richardson-Zaki formula (2) again allows for the numerical computation of the time evolution of the particle concentration. Figure 3 shows the evolution of a particle jump settling in a linear stratification, with initial concentrations $\phi_1=0.03$ and $\phi_2=0.01$, respectively, below and above $z=12 \text{ cm}$.

If the settling speed depends on height in a nonlinear fashion, we may compute numerically the time evolution of the particle concentration and the positions of the top interface and concentration jumps. We note from Eqs. (7) that the quantity $K_2 = U_s \phi (1 - \phi)^{5.1}$ remains constant along characteristics given by $dz/dt = -U_s d[\phi(1 - \phi)^{5.1}]/d\phi$. From a given initial particle concentration, we may thus solve numerically for ϕ . If a discontinuity occurs and is such that the concentration above the shock, ϕ_a , is less than that below, ϕ_b , the settling process is expected to remain stable. If the concentration of particles is everywhere less than 15% , the concentration jump remains sharp and the speed of the shock is given by Eq. (10). Computing the concentrations of the bottom and top regions using the method of characteristics, we may track the position of the concentration jump as a function of time. The speed of the top interface obeys Eq. (16), which may also be integrated in time, using $z_i(0) = h$.

III. CONVECTIVE INSTABILITIES

We consider a physical system where an initial particle concentration $\phi_i(z)$ settles in a fluid whose density increases with depth, $d\rho_f/dz < 0$. If particles are denser than the ambient fluid, $\rho_p > \rho_f$, a vertical gradient in particle concentration may yield a statically unstable density gradient and may give

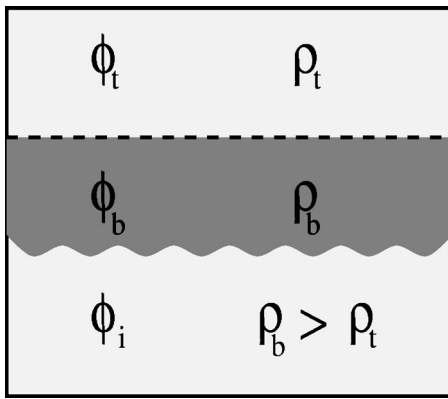


FIG. 4. If particles settle through an ambient density jump, $\rho_t < \rho_b$, instabilities may develop if the concentration below the jump is greater than the initial concentration in the bottom region $\phi_b > \phi_i$.

rise to large-scale convective overturning. We derive in this section a criterion for the development of a statically unstable bulk density profile from particles settling in a stably stratified ambient.

A simple criterion may be obtained for the formation of an unstable density profile from sedimentation across a stable density jump. Consider a fluid of density ρ_t containing an initial particle concentration ϕ_t overlying a fluid of density ρ_b and particle concentration ϕ_i (see Fig. 4). Conservation of particle flux across the interface requires that the concentration of particles having settled through the jump, ϕ_b , satisfies

$$\phi_b f(\phi_b) = \frac{\phi_t f(\phi_t)(\rho_p - \rho_t)}{(\rho_p - \rho_b)}. \quad (18)$$

If $\phi_b > \phi_i$, the resulting density profile is statically unstable in the lower region. In particular, if the concentration above and below the density jump are initially equal, $\phi_t = \phi_b$, the bottom region will become statically unstable owing to the development of a high particle concentration layer in its upper extremities.

We now turn our attention to systems where particles settle in a continuous, stable stratification. For example, consider a uniform concentration of particles settling in a stable density gradient overlying a region of constant density [but with no density jump, see Fig. 8(c)]. As particles settle, their concentration increases in the stably stratified region but remains constant in the region of constant density. A region of high particle concentration thus forms at the top of the layer of constant density and the resulting density profile is unstable. Hindered settling facilitates the formation of such instabilities by further increasing the concentration of particles in the stratified layer. We wish to characterize the initial conditions for which an initially stable configuration may generate an unstable bulk density profile. In the following argument, we neglect hindered settling in order to obtain a simpler criterion valid to $O(\phi)$. The effects of hindered settling may be incorporated in a similar fashion but would require the use of cumbersome notation.

We begin by recalling that, in the absence of hindered settling, the quantity $K_2 = U_s \phi$ is constant along characteris-

tics of slope $dz/dt = -U_s(z)$. We define a function $a(z) = \int_0^z (U_s(z'))^{-1} dz'$ such that characteristics passing through a point (z, t) originate from the point $(z_0, 0)$, with

$$a(z_0) = a(z) + t. \quad (19)$$

The concentration of particles at any point (z, t) below the top interface is then

$$\phi(z, t) = \frac{U_s(z_0)\phi_i(z_0)}{U_s(z)} = \frac{U_s(a^{-1}(a(z) + t))\phi_i(a^{-1}(a(z) + t))}{U_s(z)} \quad (20)$$

where ϕ_i is the initial particle concentration.

Because the settling speed changes only owing to variations in the ambient fluid density, $\rho_f(z)$, we have

$$\frac{U_s(z_0)}{U_s(z)} = \frac{\rho_p - \rho_f(z_0)}{\rho_p - \rho_f(z)}. \quad (21)$$

The density of the suspension then becomes, according to (20) and (21),

$$\begin{aligned} \rho(z, t) &= \rho_f(z) + \phi(z)(\rho_p - \rho_f(z)) \\ &= \rho_f(z) + \phi_i(z_0)(\rho_p - \rho_f(z_0)). \end{aligned} \quad (22)$$

Using the definition of $a(z)$ and Eq. (19) we find the derivative of the density of the suspension to be

$$\begin{aligned} \left. \frac{d\rho}{dz} \right|_z &= \left. \frac{d\rho_f}{dz} \right|_z + \frac{\rho_p - \rho_f(z_0)}{\rho_p - \rho_f(z)} \left((\rho_p - \rho_f(z_0)) \left. \frac{d\phi_i}{dz} \right|_{z_0} \right. \\ &\quad \left. - \phi_i(z_0) \left. \frac{d\rho_f}{dz} \right|_{z_0} \right) \end{aligned} \quad (23)$$

A simple result may be found if we further assume that the initial concentration of particles is uniform. We then find that an unstable density profile, $d\rho/dz > 0$, is formed at a height z if

$$\left. \frac{d\rho_f}{dz} \right|_z > \phi_i(z_0) \left(\frac{\rho_p - \rho_f(z_0)}{\rho_p - \rho_f(z)} \right) \left. \frac{d\rho_f}{dz} \right|_{z_0} \quad (24)$$

where it should be noted that the derivative of ρ_f with respect to z is everywhere negative (or zero). For a given z , $z_0(t)$ ranges over all values such that $h > z_0 > z$. In particular, if the density gradient vanishes ($d\rho_f/dz = 0$) beneath a stratified region, particle settling will always result in a statically unstable density profile. This criterion also indicates that no statically unstable profile may develop due to particle settling if the fluid density gradient becomes more negative with increasing depth ($d^2\rho_f/dz^2 > 0$). We note that larger particle concentrations will more readily generate unstable density profiles, which is to be expected since particles act as the destabilizing agent.

The analogy with the Rayleigh-Bénard instability suggests that the formation of a statically unstable density profile does not necessarily lead to large-scale convective overturning. In particular, both fluid viscosity and the downward propagation of the particle concentration gradient due to particle settling may act to stabilize the system: Perturbations must presumably grow faster than the particle settling speed in order for instabilities to develop.²⁹ The vertical extent of

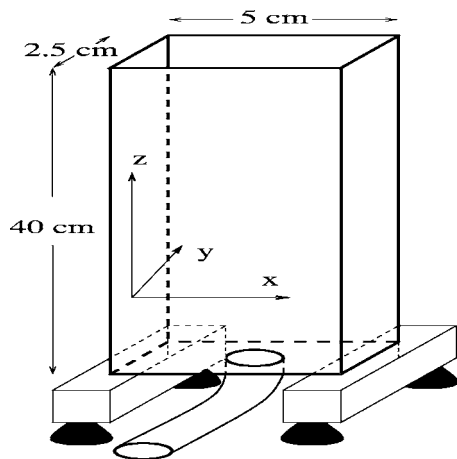


FIG. 5. A schematic illustration of the apparatus used in our experimental study. The tank is filled from below via the Oster double-bucket technique to obtain a stably stratified ambient with either a suspension of uniform concentration or a particle concentration jump.

the unstable region, $d(t)$, typically grows as particles settle and we may define a time-dependent Rayleigh number

$$\text{Ra}(t) = \frac{g\Delta\rho d(t)^3}{\rho\kappa_\phi\nu} \quad (25)$$

where $\Delta\rho$ is the density difference across the unstable region. If $\text{Ra}(t)$ exceeds a critical value, perturbations to the concentration profile will grow, under the influence of gravity, at a rate larger than both the diffusive and particle settling rates and convective motions will dominate the system. The onset of instability is therefore expected to coincide with the unstable region reaching its critical size.

If convective motions are present, the concentration of particles becomes nonuniform across horizontal planes and the analysis of Sec. II fails. However, the horizontally averaged concentration in the convective region, ϕ_c , may be estimated using the results of Martin and Nokes.³⁰ Their analysis is based on the assumption that convective motions are sufficiently vigorous to maintain a vertically uniform averaged particle concentration. Their model may be adapted to yield the evolution of the average particle concentration in our system by assuming that this concentration is decreased by particles settling out of the mixed region and increased by particles being supplied at the top of the convective region.

IV. EXPERIMENTS

A series of experiments were conducted in order to investigate the evolution of a suspension settling in a stably stratified ambient. Particular attention was given to tracking the position of the top interface and concentration jumps and to examining the stability of the resulting motion. The experimental apparatus, shown schematically in Fig. 5, consisted of a Plexiglas tank 40 cm high, 5 cm wide, and 2.5 cm thick. Vibration control mounts isolated the container from mechanical disturbances and were used to level the system and so ensured that no Boycott effect was present.³¹ Bangs Labs polymer beads of density 1.19 g/cc and radius

$49 \pm 8 \mu\text{m}$ were used and the smallest particles present, with radius $41 \mu\text{m}$, determined the progression of the top interface.

Salt water was used as a suspending fluid and linear density gradients were generated via the double-bucket technique.³² Nonlinear density gradients could be generated by varying the flow rates between the two buckets. The container was filled from below with progressively heavier fluid. Two distinct initial particle distributions were considered. To produce an initially uniform distribution of particles, an equal volume fraction of particles was added to each of the two source buckets. To produce a system marked by an initial particle concentration jump, a given volume fraction of particles was initially present in each source bucket; at the appropriate time, particles were added simultaneously to both buckets so that the concentration increased abruptly and remained constant thereafter. The filling process took approximately one minute, in which time particles settled less than 2 cm.

In our experiments, the hydrodynamic particle diffusivity is very small,³³ $\kappa_\phi \sim 10^{-8} \text{m}^2/\text{s}$, and the associated Péclet number is thus approximately $\text{Pe} = u_s h / \kappa_\phi = 10^4$. Particle diffusion therefore only plays a role near particle concentration discontinuities and over scales of order 0.1 mm. The effects of polydispersity also tend to diffuse shocks: Owing to particle size variations, the thickness of interfaces is expected to grow linearly in time at a rate of 5 cm/h. The propagation speed of interfaces is thus an order of magnitude faster than their spreading rate; consequently, the hyperbolic model will adequately provide a leading order description of the evolution of the particle concentration.

Precise measurements of the density profiles were performed using a PME salinity probe calibrated using an Anton Parr DMA 35 densitometer. Because the salinity probe generated significant disruptive fluid motion, density profiles were only taken after completion of the sedimentation process. The initial density gradient was calculated from the flow rates used in the double-bucket filling method; the reliability of these calculations was confirmed in a series of initial experiments where no particles were present. The salinity variations also prompted viscosity variations of the salt water solution³⁴ of up to 50%. From the density and viscosity profile so deduced, we could evaluate the settling speed as a function of height using Eq. (1). The settling speed typically varied by a factor of $\gamma=2$ over the depth of the tank. In the absence of large scale instabilities (see Sec. IV C), particle settling did not generate any noticeable fluid motion. The density profiles taken following the sedimentation were in good agreement with the profiles computed using the double-bucket flow rates and confirmed that the stable sedimentation process did not affect the ambient density profile.

The time evolution of concentration jumps and the top interface were measured from video recordings. The flow evolution was recorded with a Cohu 4912-2000 CCD video camera with resolution 768 by 494 pixels, and images were analyzed and enhanced with the DIGIMAGE³⁵ and MATLAB softwares. Ambient lighting was found to be the most effective, as more intense lighting led to substantial light scatter-

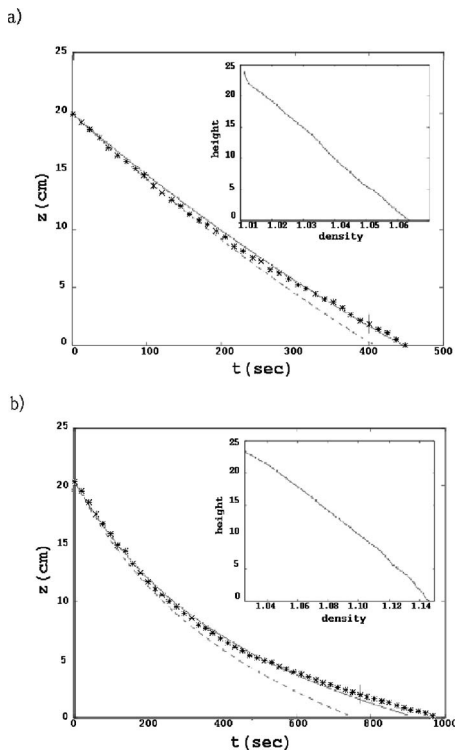


FIG. 6. Position of the top interface of a suspension with $\phi_i=1.5\%$ settling in a stratified ambient with a (a) weak ($\gamma=0.4$) and (b) strong ($\gamma=3.1$) density gradient. The dashed curves correspond to the theoretical predictions deduced by neglecting hindered settling and the solid curves are obtained by using Eq. (16). The stars indicate experimental measurements of the progression of the top interface. A typical error bar is shown. The corresponding density profile is shown on the top right.

ing and an associated loss of contrast across interfaces. The camera was located 4 m away from the container in order to eliminate parallax effects, and had a 60 by 40 cm field of view. The DIGIMAGE software allowed us to track the light intensity. The position of the top interface was tracked by tracing the evolution of a vertical slice through the fluid domain. The top interface was defined as the position where the reflected light intensity increased abruptly from a value corresponding to particle-free fluid to that of the suspension. Similarly, the position of a jump in particle concentration was defined as the position where the light intensity changed abruptly. The variations in light intensity typically occurred over a distance of several millimeters, owing principally to the polydispersity of the particles used and the associated range in settling speeds. We defined the position of the shock or top interface as the center of the transition region. The thickness of the transition region limits the accuracy with which we may determine the position of the shock, as is reflected in the error bars in Figs. 6 and 7. Qualitative observations of the particle concentration were deduced by measuring the intensity of the reflected light. Images of the convective instabilities were captured using DIGIMAGE and contrasts were enhanced using MATLAB.

A. Time evolution of the top interface

Figure 6 shows the progression of the top interface in the presence of relatively [Fig. 6(a)] weak and [Fig. 6(b)] strong

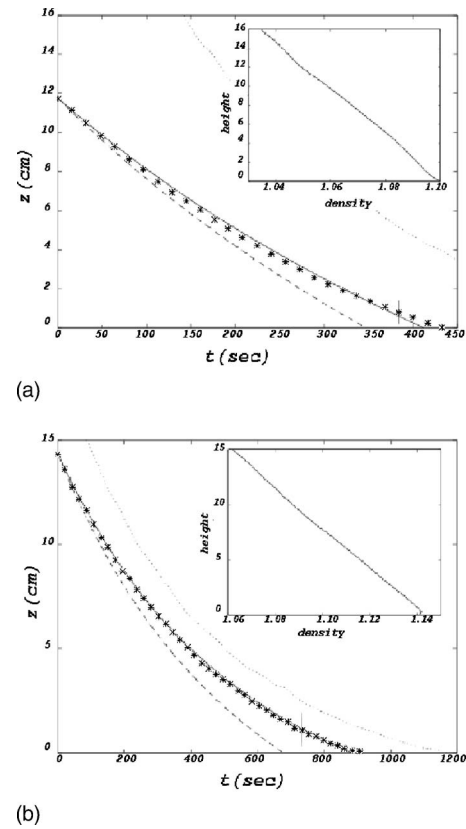


FIG. 7. Progression of a particle concentration jump, with $\phi_a=0.5\%$ and $\phi_b=2.0\%$, settling in a stably stratified ambient with a (a) weak ($\gamma=1.0$) and (b) strong ($\gamma=2.3$) density gradient. The dashed curves correspond to theoretical predictions deduced by neglecting hindered settling and the solid curves are obtained by combining Eqs. (7) and (17). The stars are experimental measurements of the progression of the concentration jump and the dotted line indicates the recorded progression of the top interface. A typical error bar is shown. The corresponding density profile is shown on the top right.

stratifications. The stars indicate experimental measurements while the solid line was computed via Eq. (16). Computations deduced through the neglect of hindered settling are also plotted as the dashed line for the sake of comparison. In both experiments, the initial particle concentration is 1.5%. In the case of a weak stratification [$\gamma=0.4$, Fig. 6(a)], the ambient stratification is predicted to cause the particle concentration to increase to 2.2% by the time the suspension is completely settled out. Although no quantitative measurements could be made of the particle concentration, variations in the reflected light intensity indicated that ϕ increased appreciably as the particles settled. For small values of γ , the total settling time may be predicted to within an error of approximately 5% by neglecting hindered settling. Moreover, because the settling speed of the particles only varies by a factor of 0.4, the velocity of the top interface is nearly constant.

In the case of strong stratification [$\gamma=3.1$, Fig. 6(b)] the presence of the ambient stratification greatly affects the sedimentation process. The concentration is predicted to increase from 1.5% to approximately 5.9% by the time the interface reaches the bottom of the container. In order to describe accurately the progression of the interface, the effects of both

hindered settling and of the ambient stratification must be taken into account, as may be seen from the relatively large error (20%) obtained by neglecting hindered settling (dashed curve). The theoretical prediction (16) is seen to yield good agreement with experimental measurements for both small and large γ .

B. Concentration jump

The progression of a concentration jump is shown in Fig. 7 for particles settling in relatively [Fig. 7(a)] weak and [Fig. 7(b)] strong density gradients. In both experiments, initial particle concentrations above and below the interface are, respectively, $\phi_a=0.5\%$ and $\phi_b=2.0\%$. Computations made neglecting hindered settling are also plotted as the dashed line for the sake of comparison. The dotted line indicates the observed progression of the top interface. It may be seen in both experiments that the top interface propagates faster than the concentration jump, as one expects on the basis of Eq. (17).

For $\gamma=1.0$ [Fig. 7(a)], the ambient stratification is predicted to cause the particle concentration to increase to $\phi_a=0.9\%$ and $\phi_b=4.0\%$ by the time the concentration jump reaches the bottom of the container. As was the case for the top interface, systems with small values of γ are marked by a nearly linear concentration jump progression. Qualitative observations of the particle concentration again showed that ϕ increased significantly as settling proceeded. For $\gamma=2.3$ [Fig. 7(b)], the velocity of the concentration jump is clearly not constant and the final particle concentrations are predicted to be larger, $\phi_a=1.4\%$ and $\phi_b=5.9\%$, respectively. Neglecting hindered settling largely underpredicts the position of the concentration jump as indicated by the dashed curve in Fig. 7(b). Experimental observations are again well described by the theory of Sec. II.

C. Instability

Our experimental arrangement was such that the criterion (24) could only be qualitatively verified. In particular, the precise point where instability first develops is difficult to ascertain because of the presence of suspended particles both above and below the region of instability. The presence of instabilities was observed through the formation of large scale structures such as convective plumes and rolls that could be observed through variations in the reflected light intensity.

Particles settling in a linear density gradient or in a concave density profile, $d^2\rho_f/dz^2 > 0$, were seen to remain stable: Particles settled as individuals without generating any large scale convective motions. However, an initially uniform concentration of particles settling through a density jump was seen to give rise to particle plumes in the bottom region, in accord with previous observations.^{20,21} Initially uniform particle concentrations settling in a stably stratified ambient where the density tends to a constant toward the bottom of the tank also developed instabilities. Figure 8 summarizes the stability characteristics of the two generic density profiles.

Images were captured of the instability resulting from an

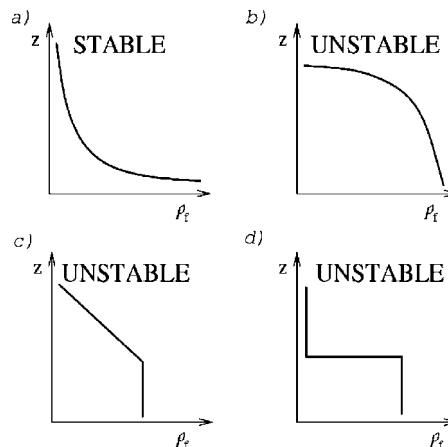


FIG. 8. A schematic illustration indicating the bulk stability of stably stratified ambients through which an initially uniform particle concentration settles. (a) If the fluid density gradient is constant or decreases with height such that (24) is satisfied, the resulting bulk density profile will remain statically stable. (b) and (c) A uniform initial particle concentration settling in a density profile such that the fluid density gradient vanishes with depth becomes statically unstable. (d) Density jumps also result in the formation of instabilities.

initially uniform concentration of particles ($\phi_i=1.5\%$) settling in a stable linear density gradient matching continuously onto an underlying region of constant density. In the early stages of the experiment, no fluid motion was observed and particles settled as individuals. The particle concentration was seen to increase in the stratified region while remaining constant in the homogeneous region. As particles settled, the particle concentration at the top of the homogeneous region came to exceed that of the bottom by an amount sufficient to prompt the formation of particle plumes. The resulting convective motions are apparent in Figs. 9 and 10. Figures 9(a)–9(c) show a region of high particle concentration (light) overlying a region of low particle concentration (dark). The initial and final density profiles are shown in Fig. 9(d); the initial profile was calculated from the double-bucket flow rates, and the final profile measured using the density probe. Although the presence of particles in both the upper and lower regions obscures them, plumes of high particle concentration, highlighted in Fig. 9(a), develop and sink. The sinking plumes arose predominantly along the sides of the container while upwelling arose in the center. Each plume contained a large number of particles and resembled those arising in generic Rayleigh-Bénard convection. Persistent regions of high and low particle concentration near, respectively, the walls and center of the container indicate the presence of a large convective roll.

The pictures shown in Fig. 9 were taken almost 10 min after the filling of the tank, by which time the particle concentration had increased significantly in the stratified region; specifically, computations suggest that the concentration in the top region should be in excess of 3% while the particle concentration in the lower region remains constant at $\phi=1.5\%$. The observed plumes typically had a diameter of 4 mm and velocity of 1 cm/s, values consistent with plumes formed through Rayleigh-Bénard instabilities driven by a density difference equal to that due to the excess particle

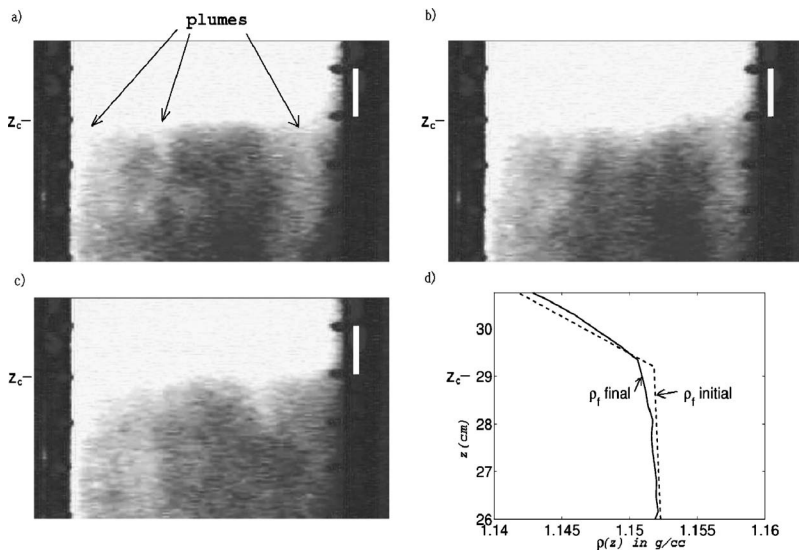


FIG. 9. The convective motion prompted by an initially uniform concentration of particles settling in a constant density gradient overlying a region of constant density. The corresponding initial and final density profiles are shown in (d). The formation of centimetric plumes beneath the critical height $z_c=29$ cm is observed. Pictures were taken at 30 s intervals and the region of high concentration is seen to remain stationary while particle plumes are shed continuously. Note that the contrasts were accentuated using MATLAB; particles are also present in the lower region. Scale bars are 1 cm.

concentration present in our system. Two counter-rotating convective rolls with typical speed 1 cm/s could also be observed, showing a vigorous upflow near the center of the container and downflow along the walls.

It may be seen in Fig. 9 that the region of high particle concentration does not progress downward. In the absence of

instability, the high ϕ region would have traveled approximately 1.5 cm between the times images [Fig. 9(a)] and [Fig. 9(c)] were captured. Instead, in the 5 min following the appearance of the first particle plumes, the region of high concentration remained stationary and shed particle plumes into the underlying region. The initial density profile [Fig. 9(d)] shows a linear ambient density gradient in the region where particles settled as individuals, $z > z_c = 29$ cm and nearly constant fluid density in the unstable region, $z < z_c$, where z_c denotes the critical height below which convection is observed. This density profile indicates that convective instability developed in the region where the density gradient vanished, in accord with criterion (24). Also, the final density profile shows that only limited mixing occurred at the top of the region of constant density; no significant entrainment of fluid from the stably stratified region was observed. Once instability was initiated, particles were transported primarily through convective rolls, with speeds that exceeded the settling speed of individual particles by an order of magnitude. The underlying region of uniform density thus appeared well mixed and the horizontally averaged particle concentration was approximately uniform for $z < z_c$.

Figure 10 illustrates the progression of the top interface [Fig. 10(a)] above and [Fig. 10(b)] through the unstable region. While in the stably stratified region, the top interface remained nearly horizontal and relatively sharp [Fig. 10(a)]. A slight tilt of the interface is observed, presumably owing to the underlying convective motion, but the interface velocity was not affected by the presence of instabilities in the lower region. However, as the top interface reached the unstable region, its downward velocity increased and exceeded the settling speed of individual particles. The interface also became increasingly diffuse and appeared significantly tilted [Fig. 10(b)] as it was distorted by convective motions.

We note that the plumes observed in our experiments are qualitatively different from those observed by Srdič-Mitrović *et al.*³⁶ In our experiments, each plume involves a large number of particles and forms because of variations in particle concentration in a fluid of nearly uniform density while

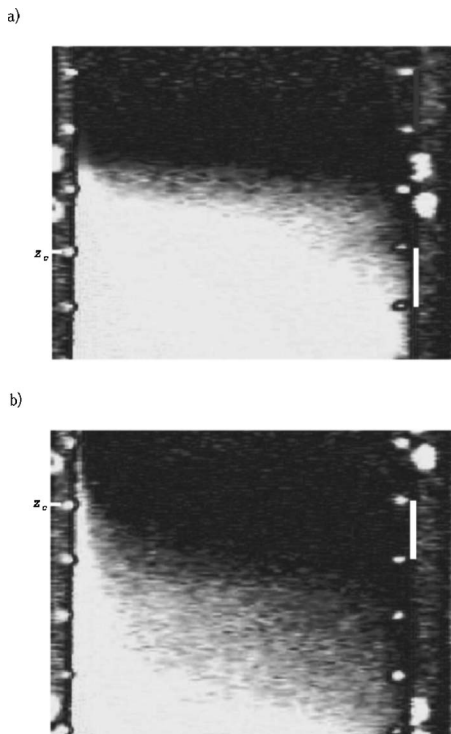


FIG. 10. Images of the top interface as it settles through (a) a stably stratified ambient in a stable region ($z > z_c$) and later through (b) a region of constant density where convective motion occurred ($z < z_c$). The initial and final density profiles are shown in Fig. 9(d). The density remains approximately constant for $z < z_c$ and decreases linearly for $z > z_c$. (a) The top interface is horizontal and relatively sharp when particles settle in a density gradient and do not generate convective overturning. (b) When the top interface reaches a region of constant density in which particles generate convective rolls, the interface becomes diffuse and tilted. Scale bars are 1 cm.

Srdič-Mitrovič *et al.* recorded plumes forming behind individual particles settling through a density interface. Here particles are not expected to entrain lighter fluid from above as their Reynolds number is less than 0.1 and the density gradient is very weak in the region where instabilities develop. The instabilities observed here are also qualitatively different from the double-diffusive instabilities that may arise when hot particle-laden fluid overlies cold particle-free fluid.³⁷ Sedimentary double-diffusive convection is characterized by millimeter scale, sparsely distributed particle fingers rather than the relatively large convective rolls observed in our experiments. Moreover, particle fingers are rapidly initiated whereas in our experiments approximately 10 min were required before the appearance of the first convective rolls. This delay suggests that the system becomes convectively unstable only after the establishment of a region of high particle concentration in a region of little or no fluid density gradient. Experimental observations thus support the relevance of the simple physical picture presented in Sec. III.

V. CONCLUSION

By generalizing the results of Kynch¹⁵ to the case of an ambient with vertical settling speed variations, we have obtained means to predict the time evolution of the concentration of particles settling in a stratified ambient. The basic scenarios of shock and expansion fan are similar to those arising in a homogeneous environment: in the dilute limit ($\phi < 15\%$), particle concentration jumps give rise to expansion fans if the lower concentration is less than the upper concentration, and travel as shocks otherwise. However, the stratified case is richer due to the time dependence of the particle concentration; specifically, the presence of a settling speed gradient causes the particle concentration to increase in time, thus enhancing the influence of hindered settling. In the case of a linear settling speed gradient, a new analytical expression (14) describing the evolution of the particle concentration was derived. The validity of the theoretical predictions describing the progression of the top interface (16) and concentration jumps (17) was verified experimentally by measuring the time evolution of a suspension of latex particles settling in salt stratified water. Good quantitative agreement was found, and the relative importance of hindered settling and ambient stratification could be readily distinguished.

In the presence of a density gradient, sedimentation may lead to the formation of convective instabilities through the development of gravitationally unstable bulk density distributions. Such instabilities modify qualitatively the physical picture described in Sec. II and dominate the time evolution of the system. We developed a criterion (24) for the stability of an initially uniform suspension settling in a stably stratified ambient. If the initial particle concentration is uniform, an unstable density gradient will form provided the magnitude of the ambient density gradient decreases sufficiently at large depth. Experiments showed good qualitative agreement with our stability criterion. A similar criterion may be obtained for cases where the settling speed variations are due to viscosity rather than density gradients. Viscosity gradients

are easily handled by replacing Eq. (21) with a corresponding expression in terms of viscosity variations

$$\frac{U_s(z_0)}{U_s(z)} = \frac{\nu(z)}{\nu(z_0)}. \quad (26)$$

Variations in settling speed resulting from variations in particle size (as may arise with chemically active particles) may be taken into account using a similar approach.

Systems where an unstable ambient density profile is stabilized by a particle concentration increasing with depth (clear, heavy fluid overlying light, particle-laden fluid) are known to become unstable as settling particles release light fluid underlying heavier fluid.³⁸ In our experiments, the ambient stratification was always statically stable so that such instabilities were not observed. The initial particle concentration profile was also statically stable, being either uniform or increasing with depth, in contrast with the experiments of Hoyal *et al.*²⁰ and Parsons *et al.*²¹ where the lower region was initially particle free. Therefore, in our experiments, particle concentration variations generated by settling through an ambient stratification were the only cause of the observed convective motions.

When an initially uniform particle concentration settles in a density gradient overlying a region of constant density, convective rolls similar to those forming in a Rayleigh-Bénard instability are observed. As noted in Sec. IV C, those instabilities are qualitatively different from double-diffusive instabilities. The particle induced instabilities observed here are characterized by relatively large, centimeter-scale plumes and may only form after particle concentration has increased sufficiently at the top of the unstable region, thus delaying their appearance. Our experimental observations, therefore, confirm that particle-driven instabilities may be a dominant feature of sedimentation in a stratified ambient even when no sedimentary double-diffusive instabilities are present.

While we derived in Sec. III criteria for the development of a statically unstable bulk profile, these will not necessarily correspond to criteria for convective instability. Convective motions are expected to dominate the transport of particles if the velocity of the convective rolls is large relative to the settling speed of particles. If both individual particles and convective motion have low Reynolds numbers, convection will be dominant if

$$\frac{U_c}{U_s} = \frac{\Delta\rho l^2}{(\rho_p - \rho_f)a^2} \gg 1 \quad (27)$$

where $\Delta\rho$ is a typical density difference over the unstable region and l is the height of the unstable region. The instability mechanism presented in Sec. III is thus potentially important as particle-laden rivers enter the oceans. As particles settle out of the fresh river water into the relatively dense, saline ocean water, their concentration increases which may cause the formation of particle plumes dominating particle transport.^{20,21} Also, suspensions settling through the thermocline in the ocean are likely to satisfy (24) once below the thermocline and the transport of particles is then expected to occur predominantly through convective rolls of particle-laden plumes.

ACKNOWLEDGMENTS

The authors thank Tom Peacock for his selfless help in setting up the experiments and Jeff Parsons for a number of valuable discussions. F.B. was supported in part by a PSG-B fellowship from NSERC and by the Schlumberger Foundation. J.B. gratefully acknowledges support from an NSF Career Grant No. CTS-0130465.

- ¹S. Friedlander, *Smoke, dust, and haze : fundamentals of aerosol dynamics* (Oxford University Press, Oxford, UK, 2000).
- ²D. Drake, "Suspended sediment and thermal stratification in Santa Barbara Channel," *Deep-Sea Res.* **18**, 763 (1971).
- ³H. E. Huppert and R. J. Sparks, "Double-diffusive convection due to crystallization of magmas," *Annu. Rev. Earth Planet Sci.* **12**, 11 (1984).
- ⁴L. Wright, "Sediment transport and deposition at river mouths: A synthesis," *Geol. Soc. Am. Bull.* **88**, 857 (1977).
- ⁵F. Azam and R. Long, "Sea snow microcosms," *Nature (London)* **414**, 495-498 (2001).
- ⁶H. Fernando, M. Lee, J. Anderson, M. Princevac, E. Pardyjak, and S. Grossman-Clarke, "Urban Fluid Mechanics: Air circulation and Contaminant Dispersion in Cities," *Env. Fluid Mech.* **1**, 1 (2001).
- ⁷H. Fischer, "Dilution of an undersea sewage by salt fingers," *Deep-Sea Res.* **5**, 909 (1971).
- ⁸J. W. M. Bush, B. A. Thurber, and F. Blanchette, "Particle clouds in homogeneous and stratified environments," *J. Fluid Mech.* **489**, 29 (2003).
- ⁹K. McMillan, P. Long, and R. Cross, "Vesiculation in Columbia River basalts in Volcanism and tectonism in the Columbia River Flood Basalts Province, S. Reicel and P. Hooper editors," *Geological Society of America Special Paper* 239, 157 (1989).
- ¹⁰A. Jenkins and A. Bombosch, "Modeling the effect of frazil ice crystals on the dynamics and thermodynamics of ice shelf water plumes," *J. Geophys. Res., [Oceans]* **100**, 6967 (1995).
- ¹¹K. Cashman, "Relationship between plagioclase crystallization and cooling rate in basaltic melts," *Contrib. Mineral. Petrol.* **113**, 126 (1993).
- ¹²E. Delnoij, F. Lammers, J. Kuipers, and W. van Swaaij, "Dynamic simulation of dispersed gas-liquid two-phase flow using a discrete bubble model," *Chem. Eng. Sci.* **52**, 1429 (1997).
- ¹³M. Essington, S. Mattigod, and J. Ervin, "Particle sedimentation rates in the linear density gradient," *Soil Sci. Soc. Am. J.* **49**, 767 (1985).
- ¹⁴G. Batchelor, *An introduction to fluid dynamics* (Cambridge Mathematical Library, Cambridge, UK, 1967).
- ¹⁵G. Kynch, "A theory of sedimentation," *Trans. Faraday Soc.* **48**, 166 (1952).
- ¹⁶G. Batchelor, "Sedimentation in a dilute dispersion of spheres," *J. Fluid Mech.* **52**, 245 (1972).
- ¹⁷J. Richardson and W. Zaki, "Sedimentation and fluidisation: Part I," *Trans. Inst. Chem. Eng.* **32**, 35 (1954).
- ¹⁸G. Oster and M. Yamamoto, "Density gradient techniques," *Chem. Rev.* (Washington, D.C.) **63**, 257 (1963).
- ¹⁹C. Völtz, W. Pesch, and I. Rehberg, "Rayleigh-Taylor instability in a sedimenting suspension," *Phys. Rev. E* **65**, 011404 (2002).
- ²⁰D. Hoyal, M. Bursik, and J. Atkinson, "Settling-driven convection: A mechanism of sedimentation from stratified fluids," *J. Geophys. Res.* **104**, 7953 (1999).
- ²¹J. Parsons, J. Bush, and J. Syvitski, "Hyperpycnal plume formation from riverine outflows with small sediment concentrations," *Sedimentology* **48**, 465 (2001).
- ²²E. Hinch, "An averaged-equation approach to particle interactions in a fluid suspension," *J. Fluid Mech.* **83**, 695 (1977).
- ²³M. Brenner, "Screening mechanisms in sedimentation," *Phys. Fluids* **11**, 754 (1999).
- ²⁴M. Ungarish, *Hydrodynamics of Suspensions* (Springer Verlag, Berlin, Germany, 1993).
- ²⁵B. J. Ackerson, S. E. Paulin, B. Johnson, W. van Megen, and S. Underwood, "Crystallization by settling in suspensions of hard spheres," *Phys. Rev. E* **59**, 6903 (1999).
- ²⁶K. E. Davis, W. B. Russel, and W. J. Glantschnig, "Disorder-to-order transition in settling suspensions of colloidal silica - x-ray measurements," *Science* **245**, 507 (1989).
- ²⁷L. Debnath, *Nonlinear Partial Differential Equations for Scientists and Engineers* (Birkhäuser, Boston, 1997).
- ²⁸S. Torquato, T. Truskett, and P. G. Debenedetti, "Is random close packing of spheres well defined?" *Phys. Rev. Lett.* **84**, 2064 (2000).
- ²⁹F. Blanchette, "Sedimentation in a stratified ambient," Ph.D. thesis, Massachusetts Institute of Technology, 2003.
- ³⁰D. Martin and R. Nokes, "Crystal settling in a vigorously convecting magma chamber," *Nature (London)* **332**, 534 (1988).
- ³¹A. Boycott, "Sedimentation of blood corpuscles," *Nature (London)* **104**, 532 (1920).
- ³²G. Oster, "Density gradients," *Sci. Am.* **213**, 70 (1965).
- ³³J. Martin, N. Rakotomalala, and D. Salin, "Hydrodynamic dispersion broadening of a sedimenting front," *Phys. Fluids* **6**, 3215 (1994).
- ³⁴*Handbook of Chemistry and Physics*, edited by R. Weast (CRC Boca Raton, Florida, 1986).
- ³⁵Software developed by Stuart Dalziel, Senior Lecturer at the Department of Applied Mathematics and Theoretical Physics of the University of Cambridge.
- ³⁶A. N. Srdič-Mitrovič, N. A. Mohamed, and H. J. S. Fernando, "Gravitational settling of particles through density interfaces," *J. Fluid Mech.* **381**, 175 (1999).
- ³⁷T. Green, "The importance of double diffusion to the settling of suspended material," *Sedimentology* **34**, 319 (1987).
- ³⁸H. E. Huppert, R. Kerr, J. Lister, and J. Turner, "Convection and particle entrainment driven by differential sedimentation," *J. Fluid Mech.* **226**, 349 (1991).